Spin-polarized band-structure calculations for Ni

J. R. Anderson
University of Maryland, College Park, Maryland 20742

D. A. Papaconstantopoulos and L. L. Boyer
Naval Research Laboratory, Washington, D. C. 20375

J. E. Schirber
Sandia Laboratories, Albuquerque, New Mexico 87115

(Received 2 March 1979)

The electronic structure of nickel as a function of the lattice constant has been studied by the self-consistent spin-polarized augmented-plane-wave method. The results confirm previous findings by Wang and Callaway regarding the different forms of the local-exchange approximation. The present calculations have incorporated the mass-velocity and Darwin relativistic effects and lead to an ordering of the energy levels at L which is consistent with photoemission measurements of Eastman *et al.* The computed changes in Fermi surface and magneton number with pressure were in reasonable agreement with corresponding measurements of the de Haas–van Alphen effect and magnetization

I. INTRODUCTION

We have performed augmented-plane-wave (APW) calculations for nickel in order to examine the effects of a change of lattice spacing on the band structure and to compare with experimental studies of the change of Fermi surface with pressure.[1,2] Previously there have been several spin-polarized band-structure calculations for nickel using different techniques including an APW calculation by Connolly[3] and the more recent studies by Callaway and Wang,[4–6] who used a linear combination of Gaussian-type orbitals. These studies have helped to determine the Fermi surface of nickel, the density of states, and the magneton number.

The present calculations were initiated because of a difficulty in explaining the changes in the Fermi surface with pressure as measured by the de Haas–van Alphen (dHvA) effect.[1,2] Two portions of the Fermi surface have been measured, the majority-spin s-p–like necks centered at L and the d-like minority spin hole pockets centered at X. In Table I the experimentally determined changes in cross-sectional areas with pressure of these two pieces are presented along with the corresponding estimates based simply upon changes in volume and magnetic moment with pressure. It can be noted that the measured changes are comparable to or smaller than the compressibility K. One might expect each cross-sectional area to increase by $\frac{2}{3}K$ if the only effect of pressure is to change the dimension of a unit cell. However, this is not the whole story. If the result of Kondorskii and Sedov[7] for the change in magnetic moment per atom with pressure (-2.9×10^{-4} kbar^{-1}) is used to estimate the transfer of carriers from spin-up to spin-down bands, and if all other changes associated with pressure are ignored, then one would predict the rather large decreases in cross-sectional area indicated in Table I in contradiction to the experimental results.

Our band-structure calculations were used to determine changes, with pressure, of the Fermi-surface cross-sectional areas and magnetic moment per atom in order to explain these differences. We found that the Fermi-surface changes were consistent with our calculated transfer of electrons between spin-up and spin-down bands and in reasonable agreement with the measurements.[1,2] The computations were carried out self-consistently for several models of exchange and correlation as described below. The von Barth–Hedin form seemed to give the best results, a

TABLE I. Estimated changes in Fermi-surface cross-sectional areas with pressure compared with experiment.

Orbit	$\frac{dA}{AdP}$ (units of 10^{-4} kbar^{-1})		
	Estimate		Experiment[a]
	M[b]	S[c]	
Necks (electrons)	−36	3.7	~6
Ellipsoids (holes)	−4	3.7	~1

[a]Reference 1.
[b]Change in area due to band repopulation based upon change in magneton number with pressure.
[c]Compressibility scaling prediction.

fact also noted by Wang and Callaway.[6] In the course of our calculations we found it necessary to perform many more iterations than were initially thought to be required in order to obtain reasonably converged values for the small cross-sectional areas of the Fermi surface. This seems to be a consequence of the spin-polarized calculation and is discussed in Sec. III.

In Sec. II the experimental techniques, especially the solid-helium phase-shift method, are summarized and in Sec. III the different calculations are described. The results and comparison with experiment are given in Secs. IV and V and conclusions are presented in Sec. VI.

II. EXPERIMENTAL TECHNIQUE

The de Haas–van Alphen frequencies were measured in single-crystal nickel spheres using the field modulation technique described previously.[1] The changes with pressure were obtained by means of the solid-helium phase-shift technique[8] in order to obtain a measurable effect. For this approach the sample is mounted in a berylium-copper pressure cell and solid helium is used to transmit the pressure. The cell is pressurized while the helium remains fluid and then the system is slowly cooled to 4 K so that the helium solidifies. At an appropriate temperature near 4 K the magnetic field is varied by a small amount relative to a fixed value so that one or a small number of dHvA oscillations can be displayed. Then the cell and sample are warmed to a temperature such that the helium melts, the pressure is changed, and the system is slowly cooled to the same temperature as before. Again one or a few cycles of the dHvA oscillations are displayed by the same variation of the magnetic field. From the shift of phase of the oscillations with pressure the variation of the dHvA frequency and correspondingly the variation of the extremal cross section of the Fermi surface can be determined.

III. BAND-STRUCTURE CALCULATIONS

In Fig. 1 are shown schematically the portions of the energy bands of nickel which produce the parts of the Fermi surface most susceptible to observation by means of the dHvA effect.[9] The Fermi level for "spin-up" ↑ is shifted above the Fermi level for "spin-down" ↓ by the exchange splitting ΔE. The spin-up d bands are thought to be filled which leaves only the copperlike s-p sphere with necks for the Fermi surface resulting from the spin-up bands. (There is some hybridization of spin-up and spin-down bands when spin-orbit coupling is included.)

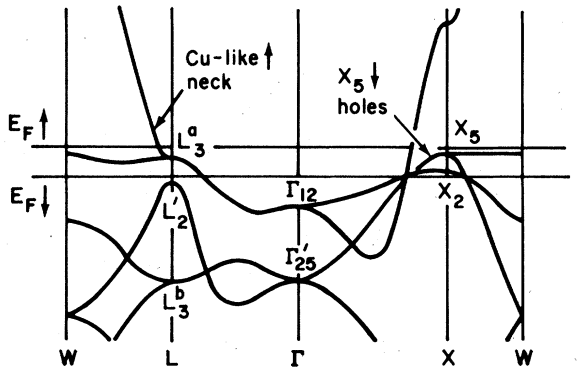

FIG. 1. Energy bands of Ni, schematic (after Gold, Ref. 9). The spin-up bands near L form the necks and the spin-down bands near X form two sets of hole pockets. The hole pockets that have been studied with the dHvA effect are formed from X_5. The spin-down Fermi level $E_F\downarrow$ has been shifted down relative to the spin-up level by a rigid exchange energy ΔE. The levels L_3^a and L_3^b refer to the upper and lower L_3 levels, respectively.

The spin-down bands form a number of Fermi surface pieces; those primarily relevant to the present discussion are the d-like hole pockets centered at X.

A. Exchange and correlation

One of the purposes of this study was to determine the contribution of exchange and correlation to these calculations. Therefore, several types of models of exchange and correlation were examined. These included:

(i) Nonrelativistic, frozen-core model with Gaspar–Kohn–Sham $\rho^{1/3}$ exchange ($\alpha=\frac{2}{3}$),[10] which we will refer to as NR.

(ii) Semirelativistic, soft-core model also with $\rho^{1/3}$ exchange and $\alpha=\frac{2}{3}$, which we will refer to as SR. For the soft-core calculations the $3s$ and $3p$ states as well as the $3d$ and $4s$ levels were calculated as bands. The lower levels were determined iteratively as atomic levels using the computer code of Liberman[11] appropriately modified to calculate charge densities corresponding to the crystal potential. The semirelativistic APW version included the Darwin and mass-velocity corrections but neglected the spin-orbit interaction. This approach, which avoids the complexity of the double group, was proposed by Mattheiss[12] and recently improved by Koelling and Harmon.[13]

(iii) Semirelativistic, soft-core model with the exchange and correlation potential constructed according to the von Barth–Hedin prescription for the local density approximation.[14] This model will be referred to as vBH. In the present work the von Barth–Hedin spin-polarized exchange and correlation potentials

were taken to be

$$V_{xc}^{+}(r_s)=\mu_{xc}(r_s)+\tfrac{1}{3}A(r_s)\left[\frac{\rho^{+}-\rho^{-}}{\rho}\right],$$

$$V_{xc}^{-}(r_s)=\mu_{xc}(r_s)+\tfrac{1}{3}A(r_s)\left[\frac{\rho^{-}-\rho^{+}}{\rho}\right],$$

where ρ^{+} and ρ^{-} are the spin-up and spin-down electron charge densities, respectively, ρ is the total electron charge density,

$$\mu_{xc}(r_s)=\beta(r_s)V_{\mathrm{KS}}(r_s)$$

and

$$A(r_s)=S(r_s)V_{\mathrm{KS}}(r_s)\ .$$

Here $V_{\mathrm{KS}}(r_s)$ is the Kohn–Sham $\alpha=\frac{2}{3}$ exchange potential.

$$\beta(r_s)=1+C_p x\ln(1+1/x)$$

and

$$S(r_s)=1+\frac{C_p}{2}y\ln(1+1/y)\ ,$$

where

$$x=\frac{r_s}{r_p}\ ,\quad y=\frac{r_s}{2^{4/3}r_p}$$

and

$$r_s=(3/4\pi\rho)^{1/3}\ .$$

Following Janak,[15] we set $C_p=0.045$ and $r_p=21.0$.

(iv) Semirelativistic, soft-core calculation with different values for α for the spin-up and spin-down bands, $\alpha\uparrow=0.728$ and $\alpha\downarrow=0.708$, as obtained from the results of Gopinathan *et al.*[16] This will be referred to as the GWB model.

B. Self-consistent APW method

The APW method that we have used to calculate spin-polarized energy bands and the Fermi surface roughly follows the approach by Connolly.[3] All calculations were carried out self-consistently within the muffin-tin approximation. The lattice constant corresponding to normal spacing was taken to be $a=3.5235$ Å, which is also the value chosen by Connolly. After each iteration the fractions of occupied spin-up and spin-down states were determined as well as the Fermi energy; these values were used in the construction of the exchange potential for the succeeding iteration.

In order to compare with pressure measurements, calculations were also made for a lattice spacing reduced by 2.5% with the NR model and by 2.5 and 5% for the vBH form of exchange and correlation. If one assumes the compressibility is constant (5.5×10^{-4} kbar^{-1}),[17] these values correspond to pressures of 135 and 270 kbar, respectively, and were thought to be large enough to give changes greater than the errors of the calculation and small enough that gross distortions in the energy bands were not expected.

For the nonrelativistic calculations the initial configurations for the spin-up and spin-down electrons were chosen as $3d^5 4s^1$ and $3d^4$, respectively, while for the relativistic calculations the initial configurations were chosen somewhat arbitrarily as $3d^{4.5}4s^{0.5}$ and $3d^4 4s^1$ for spin-up and spin-down, respectively. In all of our calculations for nickel a final spin-polarized (magnetic) system was obtained. It would be interesting to make a test of our method by carrying out similar calculations for copper. (Wang and Callaway,[5] using a nonrelativistic Hamiltonian and a slightly different value for the lattice constant, appear to have started with the same configuration for both the spin-up and spin-down states and obtained final values for the exchange splitting in nickel which were similar to ours.)

Initially the calculations were carried out self-consistently using about five iterations at six points in $\frac{1}{48}$th of the Brillouin zone and subsequently four or five more iterations at 20 points in $\frac{1}{48}$th of the Brillouin zone. It was assumed that convergence had been attained when the changes in energy levels in successive iterations were approximately 2 mRy. When we began calculating cross-sectional areas of the Fermi surface and their changes with pressure, however, we discovered inconsistencies in the values calculated. We were finally able to conclude that these errors were primarily the result of lack of convergence in our calculation. In order to discuss this, we must first describe our treatment of the constant potential outside the muffin tins.

For the standard APW calculation the constant potential outside the muffin-tin spheres is set equal to zero and all the energy levels are shifted accordingly. In the spin-polarized calculations, however, spin-up and spin-down bands are calculated separately and in each case the potential outside the muffin tin is set equal to zero. The energies of the two sets of bands, corresponding to what we call Potential 1 and Potential 2, are shifted independently and these shifts must be reconciled in order to properly position the Fermi energy. We chose to leave the energy bands calculated from Potential 1 (spin-down bands for the von Barth–Hedin form for exchange and correlation) unshifted and to shift the bands corresponding to Potential 2 by an amount $|V_{0\uparrow}|-|V_{0\downarrow}|$, where $V_{0\uparrow}$ and $V_{0\downarrow}$ are the values of the constant potentials outside the muffin tin for the spin-up and spin-down bands, respectively. After each iteration this shift was made

and then the Fermi level was determined.

The lack of convergence manifested itself particularly in the amount of the shift. Therefore, although the bands corresponding to Potential 1 appeared to be converged to better than 1 mRy, this was not the case for the Potential 2 bands. We found it necessary to iterate for the 20-point mesh a total of about 15 times in order to obtain satisfactory convergence, that is changes in all energy levels of less than 0.5 mRy for successive iterations.

After the energy bands had been converged from the 20-point mesh, a final calculation was made at 89 points in $\frac{1}{48}$ of the Brillouin zone. The Fermi surface was obtained by interpolation from this 89-point mesh except for the two small pieces, the necks at L and the hole pockets at X. In these cases the energies were calculated at $\vec{k}$ values appropriate to the 240-point mesh. Even after all this there remained small discrepancies in the values of Fermi surface areas due to numerical errors from integration and interpolation. These were most notable for the smaller cross sections and thus our results for the changes in such Fermi-surface cross sections with lattice spacing are only semiquantitative.

C. Interpolation procedures—Fermi-surface calculations

Subsequent to the final iteration, energy values were interpolated by the linear tetrahedron method,[18] starting with 89 first-principles APW points in $\frac{1}{48}$ of the Brillouin zone, to determine the density of states and its angular-momentum components, the magnetic moment per atom, Fermi-surface cross-sectional areas, and cyclotron masses. These quantities were also calculated by a Slater–Koster (SK) fit to the APW energies and the results were essentially the same as those obtained from the tetrahedron scheme. Both schemes for interpolation are described below.

In the tetrahedron approach the Brillouin zone is subdivided into tetrahedra, the corners of which correspond to $\vec{k}$ vectors at which energies have been determined from the APW calculations. Within each tetrahedron each band is interpolated linearly. That is, $\epsilon_j(\vec{k}) = \epsilon_{j0} + \vec{a}_j \cdot \vec{k}$, where $\epsilon_j(\vec{k})$ is the energy of the jth band at point $\vec{k}$, and ϵ_{j0} and the three components of $\vec{a}_j$ are parameters obtained from the known values of $\epsilon_j(\vec{k})$ at the corners of the tetrahedron. This form of interpolation is well suited to the computation of densities of states and similar functions because a single analytic expression exists for the contribution from each tetrahedron.[18] This approach can also be conveniently used for determination of the shape of the Fermi surface. The simple linear formula for each tetrahedron, together with an appropriate scheme for selecting the correct tetrahedron in the fundamental Brillouin zone corresponding to an arbitrary $\vec{k}$ vector provides an efficient algorithm for specifying $E(\vec{k})$ for all $\vec{k}$. The linear expressions for adjacent tetrahedra become identical at their common cell boundaries, and therefore the interpolated band structure is continuous from one cell to the next. Once $\epsilon_j(\vec{k})$ is determined for all bands j it is a straightforward matter to determine the extremal cross-sectional areas of the Fermi surface and the corresponding cyclotron masses.

TABLE II. Density-of-states decomposition.

Calculation	Densities of states (Ry spin)$^{-1}$				
	$N_s(E_F)$	$N_p(E_F)$	$N_d(E_F)$	$N_f(E_F)$	$N_{\text{total}}(E_F)$
$a_0\uparrow$ NR[a]	0.1695	0.3107	1.5262	0.0006	2.2191
$a_0\downarrow$ NR[a]	0.0838	0.1708	19.1683	0.0521	19.688
$a_0\uparrow$ SR[a]	0.1832	0.3942	1.5955	0.0070	5.3379
$a_0\downarrow$ SR[a]	0.1065	0.2081	20.0850	0.0429	20.6680
$a_0\uparrow$ vBH[a]	0.1913	0.4098	1.7130	0.0074	2.5762
$a_0\downarrow$ vBH[a]	0.1017	0.1983	21.3050	0.0430	21.8732
$a_0\uparrow$ vBH[b]	0.2751	0.4396	(1.1470[c]—2.542[d])		2.116
$a_0\downarrow$ vBH[b]	0.2249	0.2058	(14.435[c]—6.080[d])		20.940
0.975 $a_0\uparrow$ vBH[a]	0.1660	0.2967	1.785	0.0062	2.4487
0.975 $a_0\downarrow$ vBH[a]	0.0924	0.1844	19.420	0.0419	19.9543
0.950 $a_0\uparrow$ vBH[a]	0.1321	0.3119	1.6735	0.0076	2.3270
0.950 $a_0\downarrow$ vBH[a]	0.0849	0.1743	17.490	0.0414	18.000

[a]Tetrahedron interpolation from 89-point mesh.
[b]Slater–Koster interpolation from 20-point mesh.
[c]T_{2g} symmetry.
[d]E_g symmetry.

The Slater–Koster interpolation method was also applied in order to fit the APW energy bands from the vBH calculation at the normal lattice spacing. As parameters we used 32 interaction integrals, which include first- and second-neighbor interactions. The first six bands as well as the high-energy values at the symmetry points Γ_{15} and X_5' were fitted. These higher-energy states bring in the p character and their inclusion in the fit was found to be crucial in obtaining the correct angular-momentum decomposition of the density of states. The SK density-of-states decomposition is given in Table II to be compared with the density of states generated by the tetrahedron method. Note that the l components of the SK density of states are given for the total unit cell and not merely within the muffin-tin spheres. The l components of the electronic charge have also been calculated. The main difference between the spin-up and spin-down electrons is found in the t_{2g}-symmetry electrons.

IV. RESULTS AT NORMAL LATTICE SPACINGS

A. Energy bands

Spin-up and spin-down energy bands have been obtained for the models mentioned in Sec. III. In Fig. 2 are shown energy bands along symmetry directions in the Brillouin zone for the vBH model for the normal lattice spacing. The general features of these energy bands are representative of all our calculations. One exception was the ordering of the levels at L near the Fermi level for the spin-up bands although necks were found in each case. For example, in Fig. 3 spin-up energy levels in the vicinity of L are shown schematically for both NR and SR calculations. (Note that the same exchange was used for both these models.) The ordering of the levels from highest to lowest is L_2'-L_3-L_3 for the NR model in agreement with the calculations by Connolly[3] and Wang and Callaway[6] while for the SR and vBH models the ordering is L_3-L_2'-L_3. Consequently, in the NR case the necks are formed from the L_2' branch while in the SR and vBH cases the necks are formed from the upper L_3 branch. In Table III the energy differences between spin-up bands at L and the Fermi energy are compared for different models. Here we see explicitly that the ordering of the levels at L is different for our semirelativistic vBH calculation and the nonrelativistic vBH calculation of Wang and Callaway. Our vBH calculation and that of Wang and Callaway, except for being performed by different methods, differ only in that we include the Darwin and mass-velocity relativistic corrections. In order to determine whether these differences could account for the change in ordering, we continued iterating our nonrelativistic, ($\alpha = \frac{2}{3}$), frozen-core calculations with a soft core. The results are shown in the second column of Table III. The ordering at L is unchanged from our NR model and is the same as that of Wang and Callaway. Thus we conclude that the difference in ordering of L_2' and L_3 probably is the result of inclusion of the Darwin and mass-velocity terms in our calculations. This ordering of the levels at L from our vBH model is the same as that suggested by Eastman *et al.*[19] although the L_3 level is much closer to the Fermi energy in their

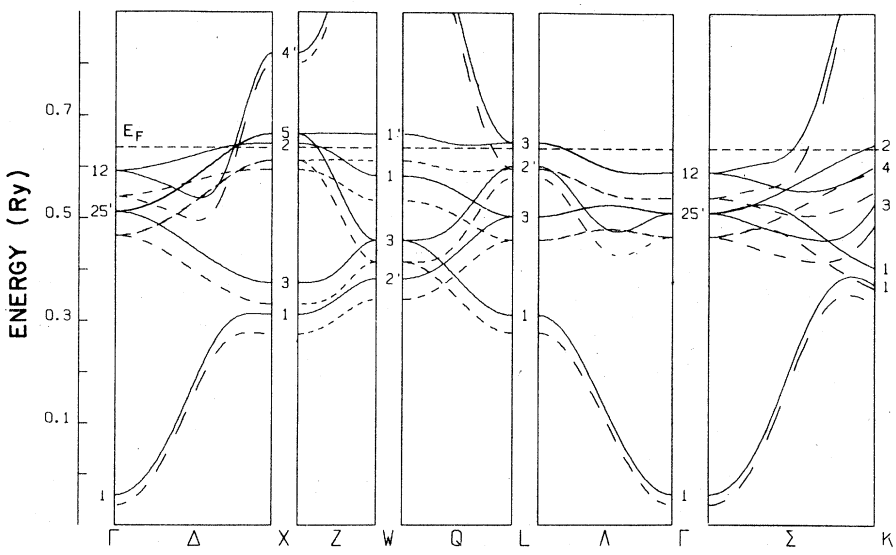

FIG. 2. Energy bands of Ni for the vBH model at normal lattice constant. The dashed lines represent the spin-up bands and the solid lines represent the spin-down bands.

TABLE III. Energy levels at L (spin-up bands).

Energies (Ry)	NR[a]	NR[b]	SR[c]	GWB[d]	vBH[e]	WC[f]	EHK[g]
E_F-E_{L_3}	0.2027	0.1938	0.1896	0.2855	0.1896	0.1709	
E_F-$E_{L_{2'}}$	0.0479	0.0298	0.0581	0.0587	0.0636	0.0278	0.062
E_F-E_{L_3}	0.0669	0.0589	0.0516	0.1600	0.0511	0.0347	0.011

[a]Non-relativistic, $\alpha=\frac{2}{3}$, frozen core.
[b]Results after eight more iterations of (a) using a soft core; nonrelativisitic, $\alpha=\frac{2}{3}$.
[c]Semirelativistic, $\alpha=\frac{2}{3}$, soft core.
[d]Semirelativistic, soft core, $\alpha\uparrow=0.728$ and $\alpha\downarrow=0.708$ (Ref. 16).
[e]Semirelativistic, soft-core, von Barth–Hedin model for exchange and correlation.
[f]Wang and Callaway (Ref. 6); von Barth–Hedin form for exchange and correlation, nonrelativistic.
[g]Interpretation of angle-resolved photoemission data, Eastman *et al.* (Ref. 19).

model ($E_F-E_{L_3}\approx 0.011$ Ry). We return to a discussion of this difference below.

The energy bands near X are shown schematically in Fig. 1; the spin-down bands based on the $X_5\downarrow$ state produce the hole pockets which give dHvA oscillations that are easily observable. Another set of hole pockets resulting from the spin-down $X_2\downarrow$ level is predicted by our calculations. Although these additional pockets have been found in all first-principles band calculations as far as we know, they have not been observed by direct experimental techniques such as measurement of dHvA effect. Such dHvA oscillations should be observable, although with difficulty, since we have calculated the cyclotron mass ratio to be about 1.9, a large value for such a small area. (Gersdorf[20] has suggested that measurements of magnetocrystalline anisotropy provide evidence for the existence of these $X_2\downarrow$ hole pockets and he estimates a much larger mass ratio of about 197.) It would be useful to search for these heavy hole pockets directly.

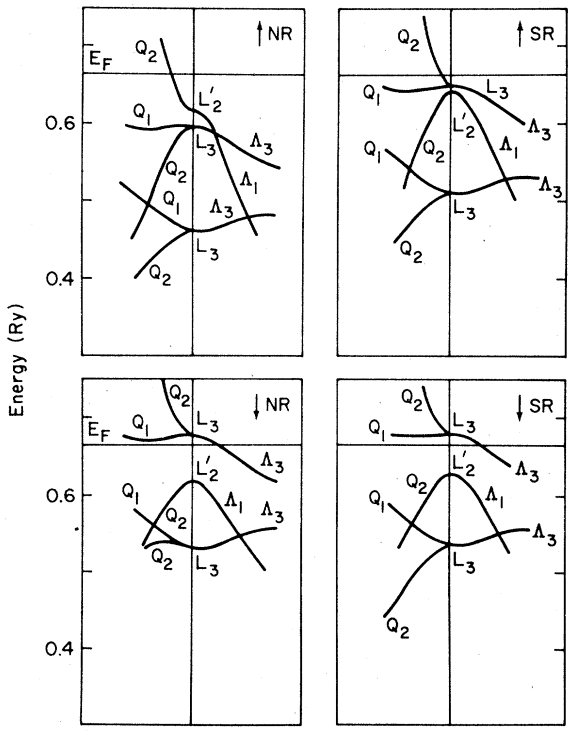

FIG. 3. Comparison of energy bands near L for the NR and SR models.

In order to compare the different models we show in Table IV energy differences which we associate with *s-p* bandwidths, *d* bandwidths, and the *s-d* separation. The *s-d* separation seems to be more sensitive to the form of the exchange and correlation than the widths of the *d* and *s-p* bands. The smallest separation *s-d* is obtained for the NR calculation, while the SR and vBH models give nearly equivalent results. For decreasing lattice spacing (increasing pressure) the bandwidths and *s-d* separation increase for all models as shown in the table. The results obtained by Wang and Callaway[6] are also shown in the table. Their bandwidths and *s-d* separation calculated with the von Barth–Hedin form for exchange and correlation are somewhat less than ours. This difference may be due to the fact that our calculation is semirelativistic. The values from our NR calculation and from the Wang and Callaway calculation ($\alpha=\frac{2}{3}$) agree fairly well. (Both these calculations were nonrelativistic.)

The exchange splittings, energy differences

TABLE IV. Comparison of energy differences (Ry).

Calculation	$E_F-\Gamma_1$	s-d separation $\Gamma_{25}'-\Gamma_1$	s-d separation $X_5-\Gamma_1$	d width X_5-X_1	s-p width $X_4'-\Gamma_1$
a_0 NR↑	0.679	0.481	0.625	0.325	0.849
a_0 NR↓	0.674	0.547	0.701	0.358	0.850
$0.975a_0$ NR↑	0.716	0.507	0.669	0.365	0.892
$0.975a_0$ NR↓	0.711	0.570	0.742	0.398	0.894
a_0 SR↑	0.701	0.518	0.664	0.334	0.862
a_0 SR↓	0.684	0.560	0.712	0.355	0.862
a_0 vBH↑	0.706	0.523	0.670	0.337	0.863
a_0 vBH↓	0.682	0.557	0.710	0.354	0.862
$0.975a_0$ vBH↑	0.747	0.549	0.714	0.377	0.907
$0.975a_0$ vBH↓	0.722	0.582	0.754	0.395	0.906
$0.950a_0$ vBH↑	0.792	0.577	0.762	0.424	0.957
$0.950a_0$ vBH↓	0.765	0.608	0.801	0.441	0.956
vBH (WC)↑[a]	0.655	0.485	0.633	0.307	0.827
vBH (WC)↓[a]	0.658	0.528	0.683	0.328	0.828
KS (WC)↑[b]	0.669	0.483	0.631	0.306	0.828
KS (WC)↓[b]	0.678	0.548	0.705	0.337	0.829

[a]Calculation of Wang and Callaway (Ref. 6) using the von Barth–Hedin form for exchange and correlation.
[b]Calculation of Wang and Callaway (Ref. 6) using the Kohn–Sham form for exchange.

between spin-down and spin-up bands, are also of interest. In Table V these splittings are presented at selected symmetry points for the NR, SR, and vBH models and compared with the results of Wang and Callaway. The splittings for the NR model are the largest but these are reduced upon iteration with a soft core as shown in the second row of Table V. The SR and vBH splittings are approximately the same and therefore we will once again discuss the vBH model as representative of our calculations. First it is clear that a rigid separation of the spin-up and spin-down bands is an inadequate approximation. Examining the points of d symmetry, L_3, Γ_{25}', and X_5, we see that the splittings vary from 57 to 64 mRy. The s-d–like points, X_1 and L_1, have a smaller exchange splitting, approximately 44 mRy. There is even a significant separation for the s- and p-like states, Γ_1 and L_2', of roughly 26 mRy.

The splittings we have calculated are somewhat larger than those obtained by Wang and Callaway who find a separation of about 44 mRy for the d states. This may be due to the fact that our vBH calculation is semirelativistic while theirs is not. Unfortunately, this does not explain the larger splittings we find for our NR model compared to Wang and Callaway's calculation with Kohn–Sham exchange. Our value for the lattice constant is larger since we have chosen the room-temperature value used by Connolly instead of a value obtained by extrapolation to $T=0$ K. A smaller value for the lattice constant, however, would increase the separations even more.

All the calculated splittings are significantly greater than recent values obtained by Eastman *et al.*[19] from angle-resolved photoemission experiments. (They estimate a splitting $E_{L_3\downarrow}-E_{L_3\uparrow}=23$ mRy.) In addition, they put the upper L_3 level much closer to the Fermi energy than we find from our studies. In order to investigate these points more fully, we considered the effect of spin-orbit coupling on the energy levels at the L point using the phenomenological approach of Hodges *et al.*[21] We have considered only L_3 states which are d-like and assumed that the spin is quantized along the [111] direction, which would be the case for a dHvA measurement of the minimum cross-sectional area corresponding to the necks at L.

From our Slater–Koster results we determined that

TABLE V. Exchange splittings.

Calculation	Energy Differences (Ry)							
	$\Gamma_1\downarrow-\Gamma_1\uparrow$	$X_1\downarrow-X_1\uparrow$	$L_1\downarrow-L_1\uparrow$	$L_2'\downarrow-L_2'\uparrow$	$L_3\downarrow-L_3\uparrow$[a]	$L_3\downarrow-L_3\uparrow$[b]	$\Gamma_{25'}\downarrow-\Gamma_{25'}\uparrow$	$X_5\downarrow-X_5\uparrow$
a_0 NR	0.0045	0.0468	0.0436	0.0028	0.0692	0.0791	0.0703	0.0799
a_0 NR	−0.0161	0.0329	0.0313	−0.0206	0.0602	0.0710	0.0616	0.0718
0.975 a_0 NR	0.0059	0.0458	0.0434	0.0045	0.0681	0.0780	0.0692	0.0792
a_0 SR	0.0166	0.0435	0.0393	0.0177	0.0569	0.0637	0.0573	0.0644
a_0 vBH	0.0239	0.0466	0.0422	0.0259	0.0570	0.0632	0.0575	0.0639
0.975 a_0 vBH	0.0251	0.0460	0.0428	0.0273	0.0576	0.0639	0.0579	0.0646
0.950 a_0 vBH	0.0268	0.0472	0.0432	0.0292	0.0576	0.0641	0.0580	0.0649
vBH (WC)[d]	−0.0033	0.0250	0.0225	−0.0039	0.0378	0.0444	0.0400	0.0463
KS (WC)[e]	−0.0094	0.0328	0.0288	−0.0106	0.0522	0.0617	0.0553	0.0645

[a]Lower L_3 level.
[b]Higher L_3 level.
[c]Soft core, eight iterations after 10 iterations of NR (frozen core).
[d]Calculation of Wang and Callaway (Ref. 6) using von Barth–Hedin form for exchange and correlation.
[e]Calculation of Wang and Callaway (Ref. 6) using Kohn–Sham form for exchange.

the lower-energy L_3 state wave functions were approximately $\frac{2}{3}$ d states of the form $(3z^2-r^2)/3^{1/2}$ and x^2-y^2 and $\frac{1}{3}$ d states of the form $(yz-xz)/2^{1/2}$ and $(2xy-yz-xz)/6^{1/2}$. For the higher-energy L_3 state the ratio was just the opposite. Therefore, we assumed that the lower L_3 states could be represented by the first two d functions and the upper L_3 states by the last two d functions. The exchange splitting ΔE was also obtained from our vBH calculation and the spin-orbit term was represented by $\xi\vec{L}\cdot\vec{S}$, where ξ was the strength of the coupling and $\vec{L}$ and $\vec{S}$ were the orbital and spin angular momenta, respectively. Details of the calculation are included in the Appendix. In Fig. 4 these exchange-split L_3 levels are plotted as a function of the strength of the spin-orbit coupling ξ. Of course, this is only an approximation to the results of a fully relativistic calculation. Nevertheless, if we assume that the Fermi level does not shift with the addition of spin-orbit coupling and that ξ has the atomic value, ~7 mRy, then the difference between E_F and $L_3\uparrow$ is reduced by about 4 mRy. This is not nearly enough since our calculated value is about 50 mRy and Eastman *et al.*[19] have interpreted their data to give a much smaller value of about 11 mRy. We have also calculated the spin-orbit splitting using perturbation theory as described by Klein and Boyer.[22] The upper L_3 levels, $L_3\uparrow$ and $L_3\downarrow$ were shifted in opposite directions each by about 6.6 mRy, which is roughly the same as our phenomenological result. (The $L_2'\uparrow$ level, which is unaffected by spin-orbit coupling in the first approximation, lies at approximately the same position as that predicted by Eastman *et al.*[19])

Moreover, even if the exchange splitting at L measured by Eastman *et al.*[19] refers to the smallest separation of spin-up and spin-down levels, split by the spin-orbit interaction, our estimate of this value would be reduced by only about 8 to 13 mRy. Therefore, spin-orbit coupling is not expected to resolve these differences. Kleinman[23] has suggested,

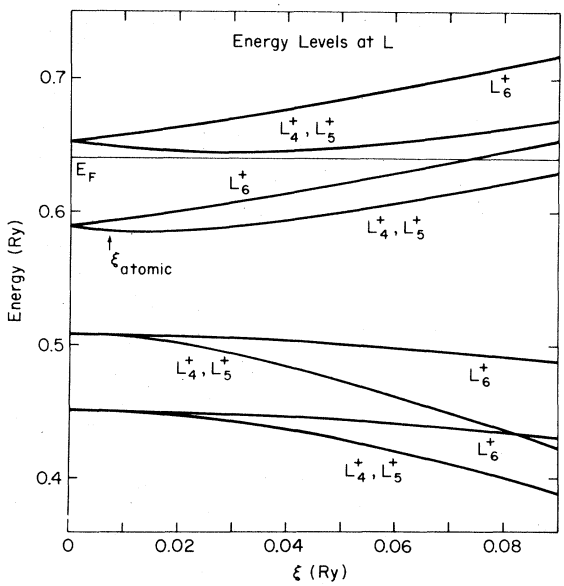

FIG. 4. Plot of L_3 levels as a function of the strength of the spin-orbit coupling ξ. The symbols L_4^+, L_5^+, and L_6^+ are the standard double-group notation at L.

TABLE VI. Core eigenvalues for vBH model.

State	Energy (Ry) Spin down[a]	Spin up
$1s$	−600.9	
$2s$	−70.7	
$2p^{1/2}$	−61.6	
$2p^{3/2}$	−60.3	
$3s(\Gamma_1)^b$	−6.871	−6.940
$3s(W_1)^b$	−6.868	−6.937
$3p(L_2')^b$	−3.980	−4.047
$3p(\Gamma_{15})^b$	−3.962	−4.030

[a]Energies are averaged for spin-down and spin-up potentials for the four lowest states.
[b]Values at selected symmetry points are given to indicate the widths of these lower (semicore) bands.

however, another explanation, that the separation between E_F and $L_3\uparrow$ will be significantly reduced by correlation effects not treated in vBH. He further shows that these effects could be large enough to reduce our calculated values for the exchange splitting to agree with the conclusions of Eastman *et al.*[19]

In Table VI for completeness we present the core energy eigenvalues from the vBH calculation. For the deepest levels the exchange splitting appears to be smaller than the errors in our calculation and therefore only the average of the spin-up and spin-down energies is given. The semicore bands, $3s$ and $3p$, are quite narrow, less than 20 mRy. The exchange splitting, however, is comparable to that for the higher bands.

B. Densities of states

The densities of states for both spin-up and spin-down bands have been obtained by interpolation using the tetrahedron and also the Slater–Koster schemes. A plot of the densities of states for the vBH model obtained from the 89-point mesh via the tetrahedron scheme is shown in Fig. 5. The three models, NR, SR, and vBH, give similar results. In Table II we present the densities of states at the Fermi energy broken up into separate angular momentum components. These values are used as input for the Gaspari–Gyorffy theory[24] for determination of λ. The total density of states at the Fermi level, 24.4 states per (atom Ry) for the vBH model, agrees with the results of Wang and Callaway[6] 22.92 states per (atom Ry), but is significantly smaller than the experimental value of 40.4 states per (atom Ry).[25] (Here we disagree with Connolly[3] who obtained a value close to the experimental result. Connolly's densities-of-states calculations, however, were based upon only 20 first-principles APW points.) From the ratio of the experimental to calculated densities of states, $1+\lambda$, we estimate an enhancement factor $\lambda \approx 0.6$. From the theory of Gaspari and Gyorffy[24] the electron-phonon interaction η has been calculated using the angular momentum components of the density of states and the scattering phase shifts, all evaluated at the Fermi energy. Our values of η and of the enhancement factor or coupling constant λ ($=\eta/M\langle\omega^2\rangle$, where M is the atomic mass and ω is an appropriate phonon frequency) are presented in Table VII. We have estimated $\langle\omega^2\rangle$ from the expression $\langle\omega^2\rangle = \frac{1}{2}\Theta_D^2$ where $\Theta_D = 450$ K, the experimental value for the Debye temperature for nickel.[25] The value of λ at normal lattice constant, 0.24 for vBH and 0.21 for SR, is much lower than that deduced from specific-heat measurements. We suggest that the additional enhancement results from electron-magnon interactions. We also note from Table VII the expected increase of η with pressure and the fact that the major contribution to the electron-phonon interaction is due to the spin-down electrons.

TABLE VII. η and λ determined by means of the theory of Gaspari and Gyorffy (Ref. 20).

Model	η (eV/Å^2) spin-up	spin-down	λ total
a_0 SR	0.05	2.17	0.21
a_0 vBH	0.06	2.44	0.24
0.975 a_0 vBH	0.07	2.85	
0.950 a_0 vBH	0.11	3.38	

From these densities-of-states calculation we have also determined the magneton numbers, $n\uparrow - n\downarrow$, for nickel. (See Table VIII.) These values are 0.69 and

TABLE VIII. Magneton number and change with pressure.

	Calculation NR	SR	vBH[a]	vBH[b]	Experiment
$n\uparrow - n\downarrow$	0.69	0.67	0.63	0.66	0.56[c]
$\frac{d\ln(n\uparrow - n\downarrow)}{dP}$ (10^{-4} kbar^{-1})	−2.7		−2.8		−2.94[d]

[a]Tetrahedron interpolation from 89-point mesh.
[b]Slater–Koster interpolation from 20-point mesh.
[c]Reference 26.
[d]Reference 7.

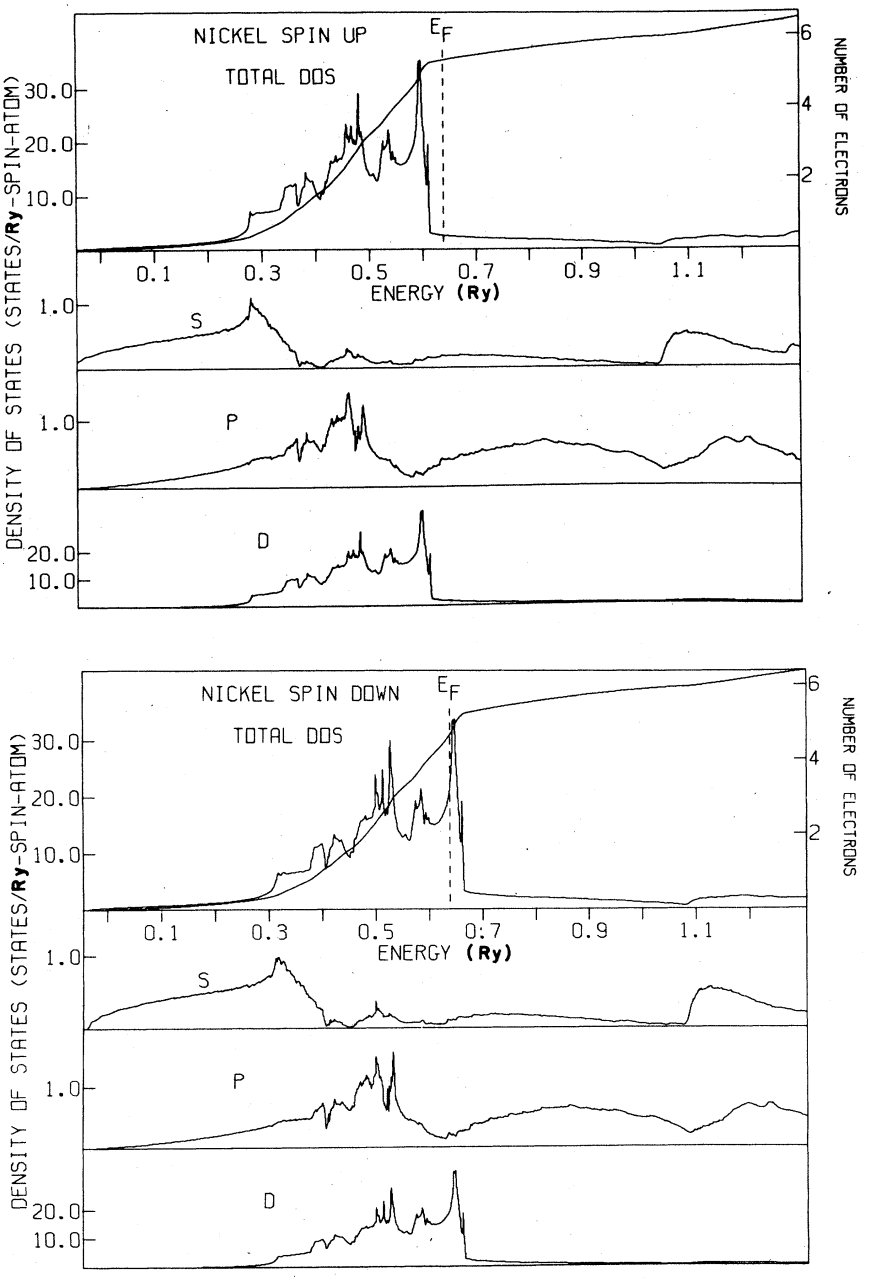

FIG. 5. Densities of states for the vBH model at normal lattice constant vs energy. The *s*, *p*, and *d* components are given separately and the totals for each spin are given by the uppermost jagged curves. The smooth curves in the upper parts of each diagram represent the number of electrons in the spin-up and spin-down bands.

0.67 for the NR and SR models, respectively, which are somewhat large but in fair agreement with the experimental value of 0.56.[26] For the vBH model the agreement is better; $n\uparrow - n\downarrow \approx 0.63$. The value obtained by Wang and Callaway, 0.58, is even closer to the experimental result. We should comment at this point that the magneton number obtained from the GWB model (different values of the exchange coefficient for spin-up and spin-down bands) was much too large, $n\uparrow - n\downarrow = 0.93$. Such a result points out the sensitivity of the magneton number to the form taken for exchange and correlation.

C. Fermi surface

The calculated Fermi surface agrees with that determined by Callaway and Wang.[4] The surface consists of: a spin-up copperlike Γ-centered surface with necks at L, two sets of spin-down hole pockets centered at X, and two large spin-down pieces centered at Γ. Not all the large portions have been observed experimentally.

Selected extremal cross-sectional areas A of the Fermi surface have been calculated for several of our models using the approach described in Sec. III and these areas are compared with those of Wang and Callaway[5] and with dHvA experimental values in Table IX. The dHvA frequencies F have been converted to cross-sectional areas by means of the relation

$$F(\text{Gauss}) = A\,(\text{a.u.}^{-2}) \times 3.741 \times 10^{8} \ .$$

From the table it can be noted that the agreement between calculation and experiment is good for the larger pieces of the Fermi surface. Even for the X-centered hole pockets the models agree fairly well with the dHvA results if one takes into consideration the fact that the shapes of the pockets depend upon the direction of the applied magnetic field used in dHvA experiments.[21] For the smallest pieces, the necks at L, the agreement is not very good. The NR model gives especially poor values, but even the cross-sectional area predicted by the vBH model is about three times the experimental value. This discrepancy is probably connected with the position of the upper L_3 level relative to E_F. Since the addition of the spin-orbit interaction does not significantly shift L_3 relative to E_F, we do not expect that a fully relativistic calculation would substantially improve the agreement. As we mentioned earlier, Kleinman[23] has suggested that correlation effects will significantly decrease the separation between E_{L_3} and E_F. We would expect a similar decrease in the neck cross-sectional area and therefore we expect correlation effects to account for the discrepancy between calculation and experiment, at least partially.

TABLE IX. Cross-sectional areas of the Fermi surface.

Orbit	Orientation	Center	Band	A (a.u.$^{-2}$)						m^*/m_0	
				WC[a]	NR	vBH[b]	vBH[c]	Expt.	vBH[c]	WC[a]	Expt.
Necks	[111]	L	6↑	0.0068[d]	0.043	0.035	0.0236[e]	0.0071[f]	0.17		0.22[f,h]
Necks	[110]	L	6↑				0.0402[e]	0.0102[f]	0.29		0.36[f]
Necks	[112]	L	6↑				0.0313[e]				
Large Square	[001]	Γ	6↑	1.24		1.25	1.23	1.15[g]	1.95	2.22	
Pockets	[001]	X	3↓	0.018	0.041	0.020	0.023[e]	0.0267[f]	0.90	0.66	0.77[h,i]
Pockets	[100]	X	3↓	0.038	0.079	0.048	0.049	0.0665[f]	1.41		
Pockets	[111]	X	3↓			0.0294	0.028	0.0442[f]			
Pockets	[110]	X	3↓		0.073	0.045	0.034	0.0585[f]	1.69		
Pockets	[101]	X	3↓				0.028				
Pockets	[001]	X	4↓	0.089		0.059	0.050		1.59	1.97	
Pockets	[100]	X	4↓	0.144		0.101	0.086		2.24		
Pockets	[110]	X	4↓			0.086	0.070		1.51		
	[001]	Γ	5↓	2.20		1.96	2.04		9.53	8.84	
	[110]	Γ	5↓			1.56	1.59		8.06		
	[111]	Γ	5↓			2.03	2.08		11.41		
small square	[001]	Γ	6↓	0.84		0.84	0.80	0.9[g]	3.45	4.75	4.33[i]
	[110]	Γ	6↓			1.00	0.96		4.62		
	[111]	Γ	6↓			0.79	0.71		3.23		

[a]Reference 5.
[b]Slater–Koster interpolation from 20-point mesh.
[c]Tetrahedron interpolation from 89-point mesh.
[d]Callaway and Wang (Ref. 4). We have assumed that there is a misprint in this paper.
[e]Tetrahedron interpolation from equivalent of 240-point mesh.
[f]Reference 28.
[g]Data obtained by R. W. Stark as reported in Ref. 5.
[h]Reference 27.
[i]Goy and Grimes, see Ref. 29.

V. RESULTS AT REDUCED LATTICE SPACINGS

We have calculated the energy bands, Fermi-surface cross sections, densities of states, and magneton numbers for lattice spacings reduced by 2.5% with the NR model and by 2.5 and 5% with the vBH model. Changes with lattice spacing have been converted to changes with pressure by using the experimental value for compressibility of nickel[17] and the results are summarized in Tables VIII (magneton number) and X (cross sections of the Fermi surface). The pressure derivatives presented in Table X are the average from calculations at 2.5 and 5% reduction in lattice spacing. For the necks and the hole pockets after five iterations with the 20-point mesh the results for 2.5 and 5% reduced lattice constants were inconsistent. It was necessary to make about ten more iterations with the 20-point mesh at each lattice spacing in order to obtain an approximately uniform variation of cross-sectional area with lattice spacing as described in Sec. III. The neck and hole pocket cross sections were calculated from points corresponding to a 240-point mesh while the larger pieces of the Fermi surface were found from the 89-point mesh.

The calculated pressure derivatives of the extremal cross-sectional areas of the necks and hole pockets (Table X) are small, in qualitative agreement with the dHvA measurements.[1,2] Our calculations suggest that the experimental pressure derivative of the (001) hole-pocket cross-sectional area of the Fermi surface is positive in contradiction to the negative value reported by Vinokurova *et al.*[2] We believe that our solid-helium phase-shift measurements for this piece of Fermi surface are very reliable. (There are no pressure data for the larger pieces.) In addition there is very good, possibly somewhat fortuitous, agreement between our calculated change in the magneton number with pressure (-2.8×10^{-4} kbar^{-1}) and that measured by Kondorskii and Sedov[7] (-2.94×10^{-4} kbar^{-1}).

It does not seem to be possible to explain the changes in these cross-sectional areas of the Fermi surface with pressure on the basis of a simple model. The simple model of Svechkarev *et al.*[30] based on parameters for the relative shift of *s-p* and *d* bands and the redistribution of electrons among the bands does not fit the experimental results. However, from our band calculations for the neck orbit and hole pockets, we obtain magnitudes for the pressure derivatives that are in agreement with experiment and much smaller than one would expect based merely on a shift of electrons from spin-up to spin-down bands

TABLE X. Pressure derivatives of cross-sectional areas of the Fermi surface.

Orbit	Orientation	Center	Band	$\frac{d \ln A}{dP}$ (units of 10^{-4} kbar^{-1}) Calc.[a]	Expt.
Neck	[111]	L	6↑	2.6[b]	6.0[c](8.0[d])
Neck	[110]	L	6↑	1.5	
Neck	[112]	L	6↑	2.3	(6.6[d])
Large Square	[001]	Γ	6↑		
Pockets	[001]	X	3↓	2.6[b]	1.0[c](−0.8[d])
Pockets	[100]	X	3↓	3.1	
Pockets	[110]	X	3↓	2.6	
Pockets	[101]	X	3↓	2.5	
Pockets	[112]	X	3↓		(1.5[d])
Pockets	[111]	X	3↓	2.7	(6.6[d])
Ellipsoids	[001]	X	4↓	−0.4	
	[100]	X	4↓	1.4	
	[110]	X	4↓	1.9	
	[001]	Γ	5↓	4.4	
	[110]	Γ	5↓	4.5	
	[111]	Γ	5↓	4.5	
Small Square	[001]	Γ	6↓	4.3	
	[110]	Γ	6↓	4.0	
	[111]	Γ	6↓	4.3	

[a]Calculated from the vBH model using tetrahedron interpolation from the 89-point mesh.
[b]Calculated from equivalent of 240-point mesh.
[c]Solid-helium phase-shift technique.
[d]Reference 2.

TABLE XI. Separation of hole pocket and neck energy levels.

Calculation	Energy (Ry)[a] $X_5\downarrow$-$L_2'\uparrow$	$X_5\downarrow$-$L_3\uparrow$
a_0 NR	0.0753	
0.975 a_0 NR	0.0903	
a_0 SR		0.0793
a_0 vBH		0.0789
0.975 a_0 vBH		0.0815
0.950 a_0 vBH		0.0838

[a]Choice of L_2' or L_3 corresponding to the energy band forming the necks.

as discussed in Sec. I.

In Table XI we show the energy differences, $X_5\downarrow$-$L_2'\uparrow$ for NR and $X_5\downarrow$-$L_3\uparrow$ for SR and vBH, for normal and reduced lattice spacings as a partial indication of the shift of electrons between necks and ellipsoids. We see that the difference actually increases with increasing pressure. This result by itself might suggest that there is a transfer from spin-down to spin-up bands with increasing pressure or in other words that the estimates based upon only the change in magneton number with pressure are incorrect. Therefore we see that the pressure effects are quite subtle. The appropriate energy levels $X_5\downarrow$ and $L_3\uparrow$ (or $L_{2'}\uparrow$ for NR) shift away from the Fermi energy with increasing pressure, but the energy also changes more quickly with wave vector (decrease in mass). Consequently the bands cross the Fermi level at nearly the same k values as in the normal pressure case and the cross-sectional areas of the ellipsoids and necks are little affected by pressure.

VI. CONCLUSIONS

We have compared several different treatments of exchange and correlation in our spin-polarized APW calculations for nickel. We have found that the von Barth–Hedin model gives somewhat better results for the magneton number and Fermi surface than the $\alpha=\frac{2}{3}$ model, a fact also noted by Wang and Callaway. A large enhancement in the density of states, over and above that due to phonons, has been obtained and we conjecture that electron-magnon interactions contribute significantly to this enhancement.

The ordering of the energy levels at L appears to change with the inclusion of the Darwin and mass-velocity relativistic corrections to the Hamiltonian although the effect is very small. That is, near the Fermi level $L_2'\uparrow < L_3\uparrow$ for calculations including the relativistic terms and the order is reversed when these terms are omitted.

We also have learned that particular attention must be paid to convergence in spin-polarized calculations to obtain the accuracy required for computation of Fermi-surface changes. In order to explain measurements of Fermi-surface changes with pressure it is necessary to consider small details of the changes of the energy bands and not merely an s-d shift and a change in d-band width with pressure.

ACKNOWLEDGMENTS

We are pleased to acknowledge helpful discussions with Dr. J. W. Connolly and Dr. B. M. Klein. We wish to thank Dr. Wang and Dr. Callaway for sending us some additional details related to their calculations and we also thank Mr. William Johnson for help with some of the computations. The generous support of the University of Maryland Computer Science Center is gratefully acknowledged. This work was supported in part (J.E.S.) by the U. S. DOE under Contract No. DE-AC 04-76-DP00789.

APPENDIX: SPIN-ORBIT INTERACTION AT THE L POINT

Considering only the two L_3 levels (since there is no mixing with the L_2' states), we write the appropriate eight wave functions as

$$\psi_1=\phi_1 x_1\ ,\quad \psi_2=\phi_2 x_1\ ,\quad \psi_3=\phi_3 x_1\ ,\quad \psi_4=\phi_4 x_1\ ,$$
$$\psi_5=\phi_1 x_2\ ,\quad \psi_6=\phi_2 x_2\ ,\quad \psi_7=\phi_3 x_2\ ,\quad \psi_8=\phi_4 x_2\ .$$

Here x_1 and x_2 are the up- and down-spin wave functions quantized along [111], and the ϕ_i's, which form representations of L_3, are given by

$$\phi_1=f(r)\frac{yz-xz}{2^{1/2}}\ ,\quad \phi_2=f(r)\left[\frac{2xy-yz-xz}{6^{1/2}}\right]\ ,$$

and

$$\phi_3=f(r)(x^2-y^2)\ ,\quad \phi_4=f(r)\left[\frac{3z^2-r^2}{3^{1/2}}\right]\ .$$

Then the Hamiltonian becomes

$$\mathcal{H}=\begin{bmatrix} A & C \\ -C^* & B \end{bmatrix}\ ,$$

where

$$A=\begin{pmatrix} E_a-\frac{\Delta E_a}{2} & -\frac{i\xi}{2} & 0 & -\frac{i\xi}{2^{1/2}} \\ \frac{i\xi}{2} & E_a-\frac{\Delta E_a}{2} & \frac{i\xi}{2^{1/2}} & 0 \\ 0 & -\frac{i\xi}{2^{1/2}} & E_b-\frac{\Delta E_b}{2} & 0 \\ \frac{i\xi}{2^{1/2}} & 0 & 0 & E_b-\frac{\Delta E_b}{2} \end{pmatrix},$$

$$B=\begin{pmatrix} E_a+\frac{\Delta E_a}{2} & -\frac{i\xi}{2} & 0 & \frac{i\xi}{2^{1/2}} \\ -\frac{i\xi}{2} & E_a+\frac{\Delta E_a}{2} & -\frac{i\xi}{2^{1/2}} & 0 \\ 0 & \frac{i\xi}{2^{1/2}} & E_b+\frac{\Delta E_b}{2} & 0 \\ -\frac{i\xi}{2^{1/2}} & 0 & 0 & E_b+\frac{\Delta E_b}{2} \end{pmatrix},$$

and

$$C=\begin{pmatrix} 0 & 0 & -\frac{\xi}{2} & \frac{i\xi}{2} \\ 0 & 0 & \frac{i\xi}{2} & \frac{\xi}{2} \\ \frac{\xi}{2} & -\frac{i\xi}{2} & 0 & 0 \\ -\frac{i\xi}{2} & -\frac{\xi}{2} & 0 & 0 \end{pmatrix}.$$

Here E_a and ΔE_a represent the energy and exchange splitting, respectively, for the upper L_3 level while E_b and ΔE_b represent the same quantities for the lower L_3 level. These exchange-split L_3 levels, the eigenvalues of H, are plotted as a function of the strength of the spin-orbit coupling ξ in Fig. 4.

[1]J. R. Anderson, Peter Heimann, J. E. Schirber, and D. R. Stone, in *Magnetism and Magnetic Materials,* edited by J. J. Becker, G. H. Lander, and J. J. Rhyne, AIP Conf. Proc. 29 (AIP, New York, 1975), p. 529.

[2]L. I. Vinokurova, A. G. Gaputchenko, and E. F. Itskevich, Pis'ma Zh. Eksp. Teor. Fiz. 26, 443 (1977) [JETP Lett. 26, 317 (1977)].

[3]J. W. D. Connolly, Phys. Rev. 159, 415 (1967).

[4]J. Callaway and C. S. Wang, Phys. Rev. B 7, 1096 (1973).

[5]C. S. Wang and J. Callaway, Phys. Rev. B 9, 4897 (1974).

[6]C. S. Wang and J. Callaway, Phys. Rev. B 15, 298 (1977).

[7]E. I. Kondorskii and V. L. Sedov, Zh. Eksp. Teor. Fiz. 38, 773 (1960) [Sov. Phys. JETP 11, 561 (1960)].

[8]J. E. Schirber and R. L. White, J. Low Temp. Phys. 23, 445 (1976).

[9]A. V. Gold, J. Low Temp. Phys. 16, 3 (1974).

[10]R. Gaspar, Acta Phys. Acad. Sci. Hung. 3, 263 (1954); W. Kohn and L. J. Sham, Phys. Rev. 140, A1133 (1965).

[11]D. A. Liberman, D. T. Cromer, J. T. Waber, Comput. Phys. Commun. 2, 107 (1971).

[12]L. F. Mattheiss, Phys. Rev. 151, 450 (1966).

[13]D. D. Koelling and B. N. Harmon, J. Phys. C 10, 3107 (1977).

[14]U. von Barth and L. Hedin, J. Phys. C 5, 1629 (1972).

[15]J. F. Janak, Phys. Rev. 16, 255 (1977).

[16]M. S. Gopinathan, M. A. Whitehead, and R. Bogdanovic, Phys. Rev. A 14, 1 (1976).

[17]G. A. Alers, J. R. Neighbours, and H. Sato, J. Phys. Chem. Solids 13, 40 (1960).

[18]G. Lehmann and M. Taut, Phys. Status Solidi 54, 469 (1972).

[19]D. E. Eastman, F. J. Himpsel, and J. A. Knapp, Phys. Rev. Lett. 40, 1514 (1978).

[20]R. Gersdorf, Phys. Rev. Lett. 40, 344 (1978).

[21]L. Hodges, D. R. Stone, and A. V. Gold, Phys. Rev. Lett. 19, 655 (1967).

[22]L. L. Boyer and B. M. Klein, Int. Jour. Quant. Chem. Symp. No. 9, 511 (1975).

[23]Leonard Kleinman, Phys. Rev. B (to be published).

[24]G. D. Gaspari and B. L. Gyorffy, Phys. Rev. Lett. 29, 801 (1972).

[25]M. Dixon, F. E. Hoare, T. M. Holden, and D. E. Moody, Proc. R. Soc. London Sect. A 285, 561 (1965).

[26]H. Dannan, R. Heer, and A. J. P. Meyer, J. Appl. Phys. 39, 669 (1968).

[27]J. R. Anderson, P. Heimann, W. Bauer, R. Schipper, and D. Stone, in, *Proceedings of the International Conference on the Physics of Transition Metals, Toronto, 1977,* edited by J. G. Lee, J. M. Perz, and E. Fawcett, Inst. Phys. Conf. Ser. No. 39 (IPPS, London, 1978), p. 81.

[28]D. C. Tsui, Phys. Rev. 164, 669 (1967).

[29]P. Goy and C. C. Grimes, Phys. Rev. B 7, 299 (1973).

[30]I. V. Svechkarev and V. B. Pluzhnikov, Phys. Status Solidi B 55, 315 (1973).